Quantifying Natural Light for Lighting and Display Design

Yu, C.; Pont, S.C.

DOI
10.1002/sdtp.15031

Publication date
2021

Document Version
Accepted author manuscript

Published in
International Conference on Display Technology 2021

Quantifying Natural Light for Lighting and Display Design

Cehao Yu*, Sylvia Pont*

***Perceptual Intelligence Lab (π–Lab), Delft University of Technology, Delft, The Netherlands**

Abstract

In natural scenes, the wavelength-dependent sunlight scattering in the atmosphere and the presence of occluders and mutual reflections cause variations in the local illumination's magnitude, direction, and spectral composition as a function of time and space. Yet, unlike the characterization of temporal changes of natural light, these spatial variations have received relatively limited attention. In this paper, we employed the light field concept to quantify those variations and empirically demonstrated that they are significant and how the different contributions of the diffuse and directed parts can be measured.

Author Keywords

Natural light; light field; correlated color temperature; light diffuseness

1. Introduction

The human visual system has adapted to illumination in the natural environment through biological evolution (1,2). Natural light is often assumed to benefit human wellbeing. But what is "natural light"? In everyday scenes, the light varies chromatically, spatially and directionally, which can be captured by the light field (3). The local light field describes the spectral power $E_P(\theta,\varphi,\lambda)$ arriving at a point p(x,y,z) of a three-dimensional space as a function of direction, with elevation θ ranging from 0 to π, and azimuth φ ranging from 0 to 2π, and wavelength λ ranging from about 380nm to 780nm or the visible spectrum. A typical light field consists of direct lighting from light sources and indirect lighting from (inter)reflections, refractions, scattering etc.

The spectral power distribution (SPD) of direct sunlight is more or less static, and the angular-temporal dynamics of skylight result from the indirect light originating from secondary and higher-order sources, such as, for instance, a blue sky. The light field that describes the light's spectral energy in every direction at every point in a scene captures all angular, spatial, and spectral variations.

The complex optical structure of natural light fields can be represented by a spherical harmonics (SH) series as a sum of simple functions. As shown by Mury et al. (4–6), the 0^{th}-order SH, the light density, is a scalar, namely the integration of the spectral power over the sphere. The 1^{st}-order SH corresponds with the light vector, indicating the average direction of transport of spectral power. Higher-order SH contributions refer to spatial and angular high frequencies of the light fields.

The aim of the present study was to quantify the spatial and angular variations in the natural light's illuminance level and color appearance for natural scenes by light field measurements. To this aim, we measured the light density and vector in the shade and light of several sunlit scenes under a blue sky. The light fields were captured via cubic spectral illuminance measurements (7–10). The SPDs of the light density and vector were estimated and then characterized by their magnitudes, ratio or diffuseness, and correlated color temperatures (CCT). It was found that these spatial and angular variations were large and of a similar order of magnitude as daylight variations across the day.

2. Methods

2.1. Data acquisition

We collected local light field measurements of natural outdoor scenes during daytime in July 2020 and March 2021 in Delft, the Netherlands (52.0116° N, 4.3571° E; elevation 0 m), located in the Northern hemisphere, on sunny days with a blue sky, around noon. The acquisition of local light fields was done via cubic illuminance metering (7,11–13), that is, via measurements of SPDs on six faces of a small cube centered at the point (Figure 1A). The cube was orientated so that its faces are normal to the x, y and z axes in Cartesian coordinates. The positive direction of the y axis pointed to the North, and the positive direction of the z axis faced upwards perpendicular to the ground. The SPDs were captured in spectral irradiance over a wavelength range from 380 to 780 nm in 1 nm steps by a SEKONIC c-7000 spectromaster (Figure 1B).

A total of 12 natural scenes were selected. The scenes included a variety of colored surfaces under both rural and urban settings. They were selected to contain surfaces that were partly lit by sunlight and partly in the shade so that the cast shadows formed a step or gradient. In each scene, the local light fields of the sample points in the light and shade were acquired, yielding a total of 24 local light field measurements. For illustration purposes, we also photographed all scenes via a Canon EOS 5D Mark II camera as raw images with a constant 5500K white balance.

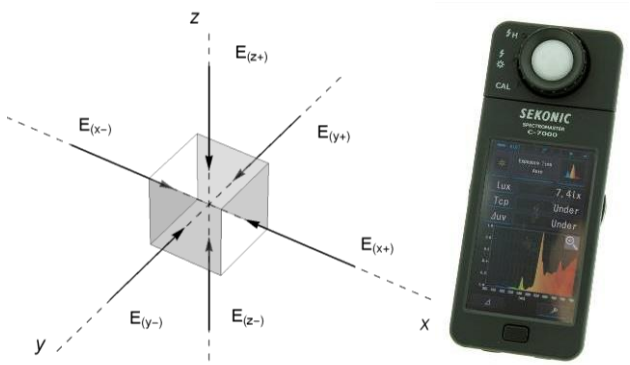

Figure 1. (A) The cubic illumination concept. (B) SEKONIC c-7000 spectral illuminance meter for SPD measurements on six faces of the cube.

2.2. Data processing and analysis

The cubic measurements $E_{(x+)}$ and $E_{(x-)}$ represent the opposed pair along the x axis, and analogous for the y and z axes. The light density can be estimated via the mean incident SPDs of the six cubic faces (14). The subtraction of the opposed paired measurements gives estimates of the light vector components in the x, y and z directions, respectively. Together these three vector components constitute the magnitude and direction of the light vector.

The SPDs of the light density and light vector weighted by the luminous efficiency function gave their spectral illuminance. The magnitudes (illuminance) of the light density and vector were calculated via integration of the spectral illuminance. Here we employed the CIE "physiologically-relevant" 2-deg photopic luminous efficiency function (15). One minus the ratio between the light vector and light density magnitudes gave the diffuseness (12).

A light probe (a white Lambertian sphere) was rendered for each measured 1st-order local light field and was superimposed on the corresponding location and photograph. A gamma value of 2.2 was applied to the linearized rendered spheres for screen display purposes.

3. Results

In Figure 2 we show results for the raw illuminance measurements, with the different faces represented on the x-axis. The connections between those measurements are just for visualization purposes and not meaningful. The light incident on the different faces of the cube had higher CCTs and much lower illuminances in the shade (left column) than in the light (right column). The angular variations were considerable, especially for the negative direction of the y axis (y-; facing south) and both directions of the z axis (z+ and z-; facing upwards and downwards, respectively). The illuminance peaks correspond with the lighting contribution from the blue sky from the top and with the sunlight direction from the south. The CCT patterns seem to correspond with the lighting contribution from the blue sky. The y- and z+ for the light condition showed relatively low CCTs combined with high illuminances, showing the strong influence from the yellowish sun (Figure 3 right column). The CCTs and illuminances for both shade and light in the z- direction (facing downward) were consistently low, measuring just (inter)reflected light from the ground.

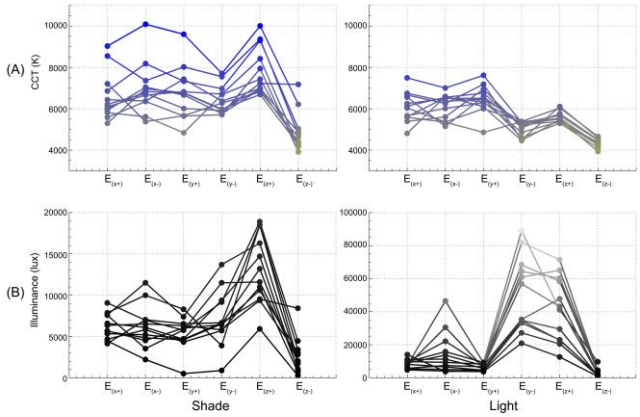

Figure 2. The CCTs (upper row) and illuminance (bottom row) of the light incidents on cubic faces in the shade (left) and light (right).

These raw results can thus be understood and explained. However, the data in Figure 2 need close scrutiny to arrive at such interpretations. Our aim is to enable intuitive fluent communication of the spatial, angular, and spectral properties of the local light field properties. To this aim we use the framework described in the introduction, which allows taking the step from working with illuminance distributions on a plane to luminance or light descriptions in a space. So we calculated the light densities and light vectors in the light and shade.

The spectral shapes of both light density and vector in the shade differed from those in the light, showing a peak in the short-wavelength part and attenuation in the long-wavelength part (Figure 3). This effect was present in all the selected natural scenes.

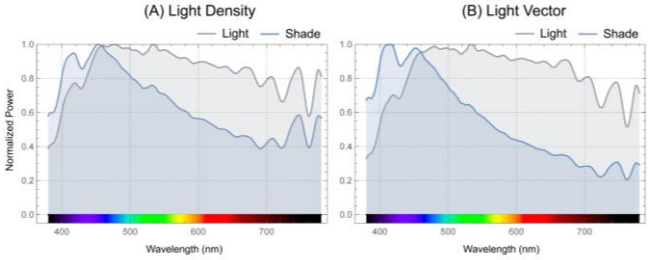

Figure 3. The normalized spectral power distributions of light density (A) and light vector (B) for the shade and light regions in scene 12.

Figure 4A shows a sample photograph of one of the scenes with the superimposed rendered spheres. We observed that the light probe in the cast shadow was bluish due to the skylight and darker than the sphere in the sun. The color of the flower (slender vervain) appeared as reddish magenta in the light but blueish purple in the shade. The step between the cast shadow and illuminated area did not just form an illumination edge but also a chromatic edge. In addition to the luminous and chromatic differences, the light probes indicate the directionality difference between sunlight and skylight (Figure 4B), which causes a difference in texture contrast (16).

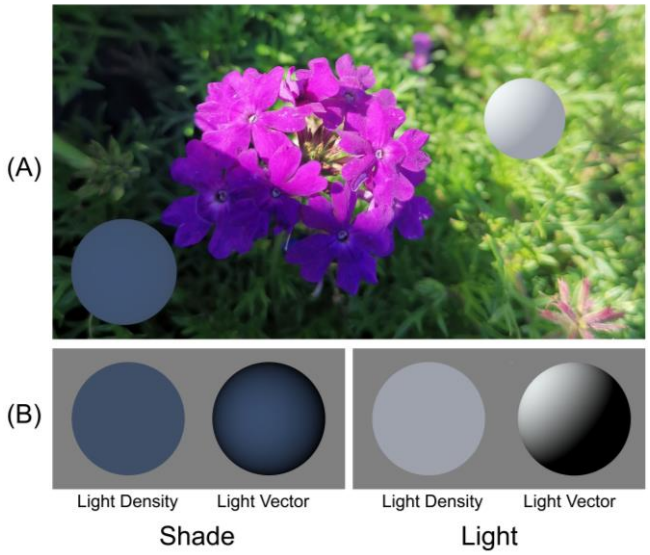

Figure 4. (A) A photograph of a sample natural scene (scene 12) with a step between shade and light. Lambertian illumination probes were rendered for 1st-order local light field approximations. (B) Order 0 and 1 approximations of local light fields.

Figure 5. The collection of all the selected natural scenes' photographs. All scenes were superimposed with light probes rendered by the local light fields. The decomposed local light fields were listed below each scene photograph in the same configuration as Figure 4. The 12 scenes were arranged from the left to the right and the top to the bottom in numerical order from 1 to 12.

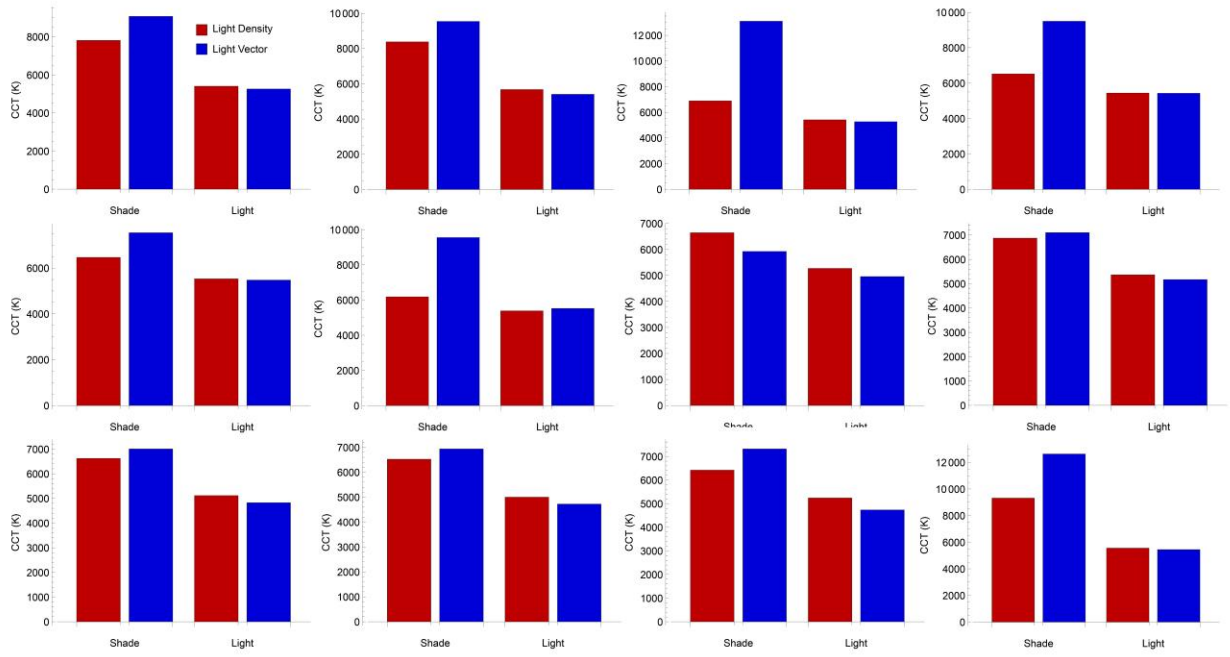

Figure 6. The CCT of the light density (red bars) and light vector (blue bars) for the shade and light regions ordered as Figure 5.

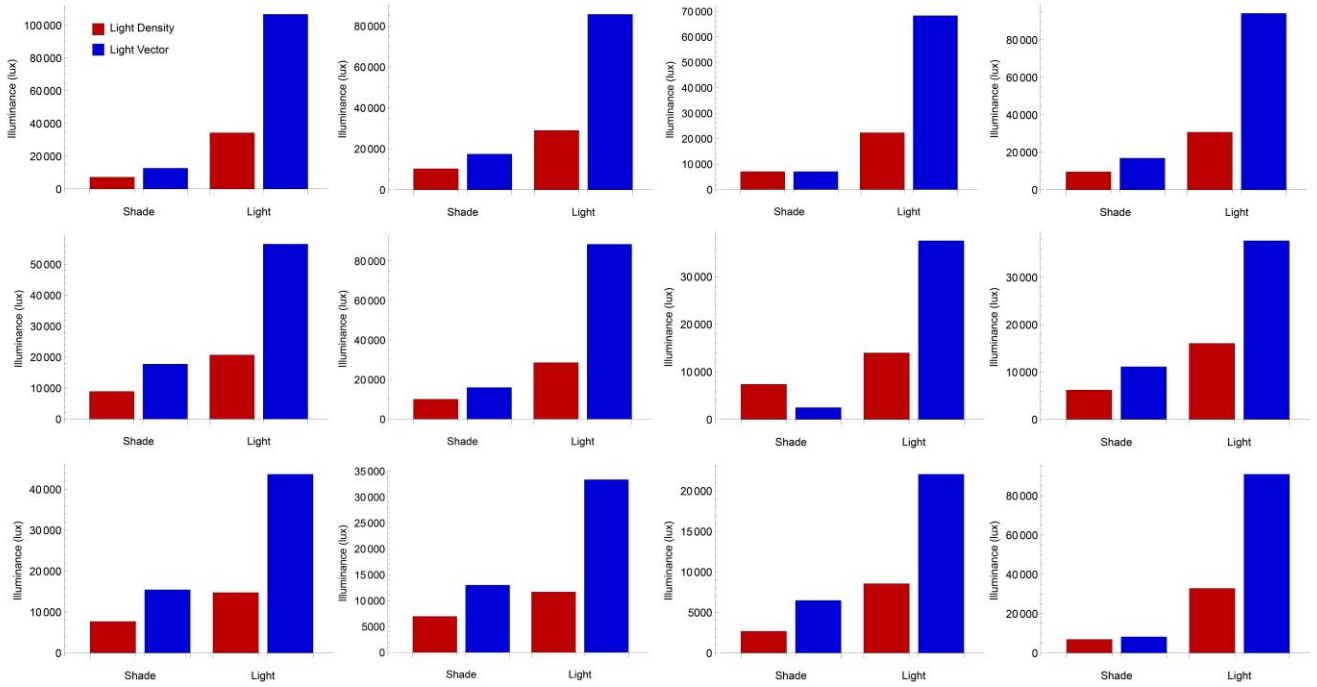

Figure 7. The magnitude in illuminance of light density (red bars) and light vector (blue bars) for the shade and light regions ordered as Figure 5.

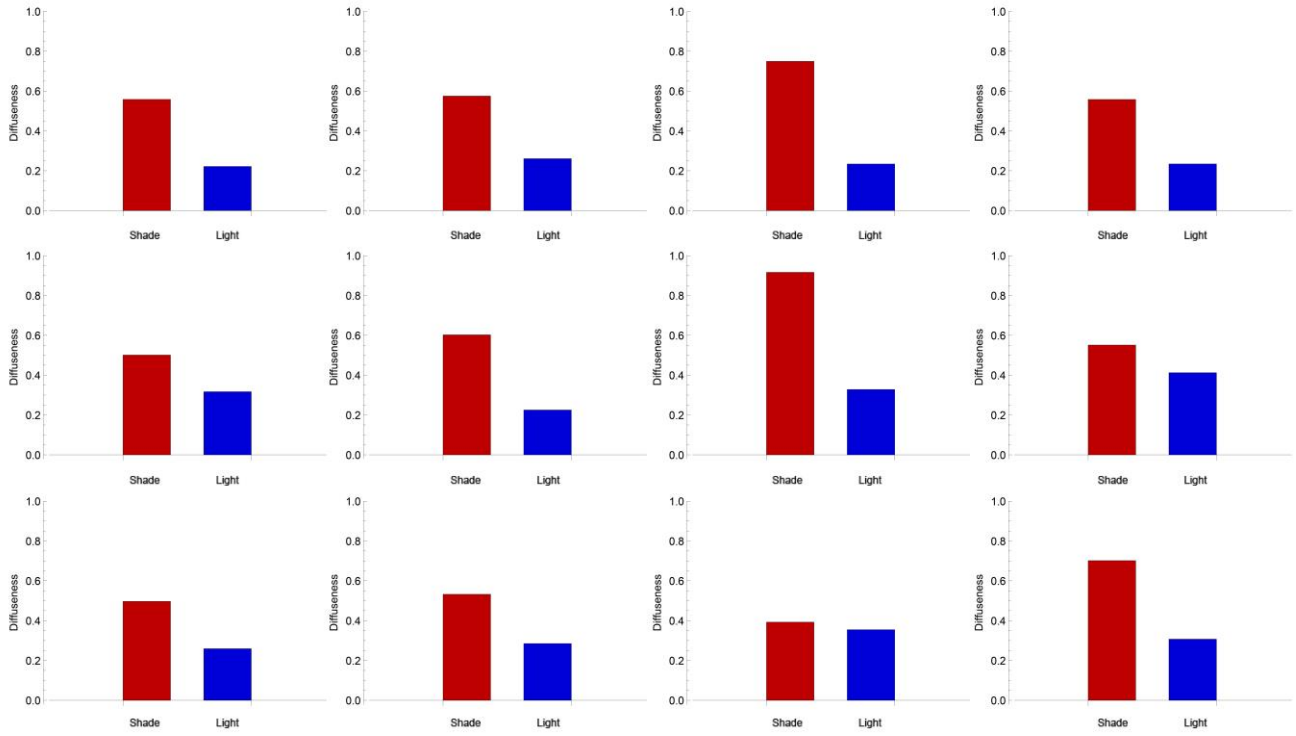

Figure 8. The diffuseness for the shade (red bars) and light (blue bars) regions ordered as Figure 5.

In Figure 5 we present the data for all 12 scenes in the same format as Figure 4. Similar effects as described above can be observed in these scenes. In Figure 6 we present the CCT for all scenes' light densities and vectors, always with the shade measurements at left and light measurements at right, as in Figure 4 and 5. The CCT of the light density in the shade was always higher (up to 3500K) than that in the light. The light vectors in shade and light had an even bigger CCT difference, up to 7200K (Figure 6). The magnitudes of the light densities and vectors, represented in Figure 7, also showed large differences in the shade and light regions, while the light vectors' differences were more prominent than for the light densities (Figure 7). The light density magnitude in the shade is relatively high compared to the light vector, resulting in high diffuseness values (0.5 – 0.9). In the light region, the light vector is much stronger than the density, resulting in a high directionality or low diffuseness values ranging from (0.2 – 0.4) (Figure 8).

4. Discussion and Conclusion

The relative contributions from low-luminance highly diffuse bluish skylight and high-luminance highly directional yellowish sunlight thus caused large magnitude and color and diffuseness differences from location to location. The light field in the shade had much lower magnitudes, bluer color appearances and higher diffuseness relative to that in the light. The spatial variations in terms of both magnitudes and color appearances were larger for the light vectors than the light densities. These spatial variations in local light field magnitude and even more the spectral properties were found to be of the same prominence as the well-known temporal variations of daylight. This study demonstrates how the light field in natural scenes can be quantified. Such data can help to design "natural light" or biophilic lighting design, using lamps and displays. Any integrated lighting and display design that mimics natural scenes thus needs to accommodate large variations in the magnitude and color and diffuseness of the resulting light.

5. Acknowledgements

This work was supported by the European Union's Horizon 2020 research and innovation programme (grant no. 765121; project "DyViTo").

6. References

1. Cronin TW, Johnsen S, Marshall NJ, Warrant EJ. Visual Ecology [Internet]. Visual Ecology. Princeton University Press; 2014. Available from: http://princeton.universitypressscholarship.com/view/10.23943/princeton/9780691151847.001.0001/upso-9780691151847
2. Koenderink J. Colour in the wild [Internet]. Traiectina: de Clootcrans Press; 2018 [cited 2020 Feb 28]. 97 p. Available from: http://gestaltrevision.be/pdfs/koenderink/
3. Gershun A. The Light Field. J Math Phys [Internet]. 1939 Apr;18(1–4):51–151. Available from: http://doi.wiley.com/10.1002/sapm193918151
4. Mury AA, Pont SC, Koenderink JJ. Structure of light fields in natural scenes. Appl Opt [Internet]. 2009 Oct 1;48(28):5386. Available from: https://www.osapublishing.org/abstract.cfm?URI=ao-48-28-5386
5. Mury AA, Pont SC, Koenderink JJ. Representing the light field in finite three-dimensional spaces from sparse discrete samples. Appl Opt [Internet]. 2009 Jan 20;48(3):450–7. Available from: https://www.osapublishing.org/abstract.cfm?URI=ao-48-3-450
6. Mury AA, Pont SC, Koenderink JJ. Light field constancy within natural scenes. Appl Opt [Internet]. 2007 Oct 10;46(29):7308–16. Available from: https://www.osapublishing.org/abstract.cfm?URI=ao-46-29-7308
7. Cuttle C. Cubic illumination. Light Res Technol [Internet]. 1997 Mar 1 [cited 2021 Apr 6];29(1):1–14. Available from: http://lrt.sagepub.com/cgi/doi/10.1177/14771535970290010601
8. Xia L, Pont S, Heynderickx I. Light diffuseness metric, Part 2: Describing, measuring and visualising the light flow and diffuseness in three-dimensional spaces. Light Res Technol [Internet]. 2017 Jun 17;49(4):428–45. Available from: http://journals.sagepub.com/doi/10.1177/1477153516631392
9. Kartashova T, Sekulovski D, de Ridder H, Pas SF te, Pont SC. The global structure of the visual light field and its relation to the physical light field. J Vis [Internet]. 2016 Aug 17;16(10):9, 1–16. Available from: http://jov.arvojournals.org/article.aspx?doi=10.1167/16.10.9
10. Pont SC. Light: Toward a Transdisciplinary Science of Appearance and Atmosphere. Annu Rev Vis Sci [Internet]. 2019 Sep 16 [cited 2019 Aug 2];5(1):7.1–7.25. Available from: https://www.annualreviews.org/doi/10.1146/annurev-vision-091718-014934
11. Yu C, Eisemann E, Pont S. Colour Variations Within Light Fields: Interreflections and Colour Effects. Perception [Internet]. 2019 Sep 16 [cited 2020 Feb 24];48:59–59. Available from: http://journals.sagepub.com/doi/10.1177/0301006619863862
12. Xia L, Pont S, Heynderickx I. Light diffuseness metric Part 1: Theory. Light Res Technol [Internet]. 2017 Jun 16;49(4):411–27. Available from: http://journals.sagepub.com/doi/10.1177/1477153516631391
13. Yu C, Pont S. Spatial and Angular Variations of Colour Rendition due to Interreflections. In: London Imaging Meeting. Springfield: Society for Imaging Science and Technology; 2020. p. xv.
14. Yu C, Pont SC. The Influence of Material Colors on the Effective Color Rendering and Temperature through Mutual Illumination. In: Color and Imaging Conference. Springfield: Society for Imaging Science and Technology; 2020.
15. Sharpe LT, Stockman A, Jagla W, Jägle H. A luminous efficiency function, V *(λ), for daylight adaptation. J Vis [Internet]. 2005 Dec 21 [cited 2021 Apr 7];5(11):3. Available from: http://journalofvision.org/5/11/3/
16. Pont SC, Koenderink JJ. Bidirectional Texture Contrast Function. Int J Comput Vis [Internet]. 2005 Apr;62(1/2):17–34. Available from: http://link.springer.com/10.1023/B:VISI.0000046587.42611.2c